JCB

Supplemental material

Mistriotis et al., https://doi.org/10.1083/jcb.201902057

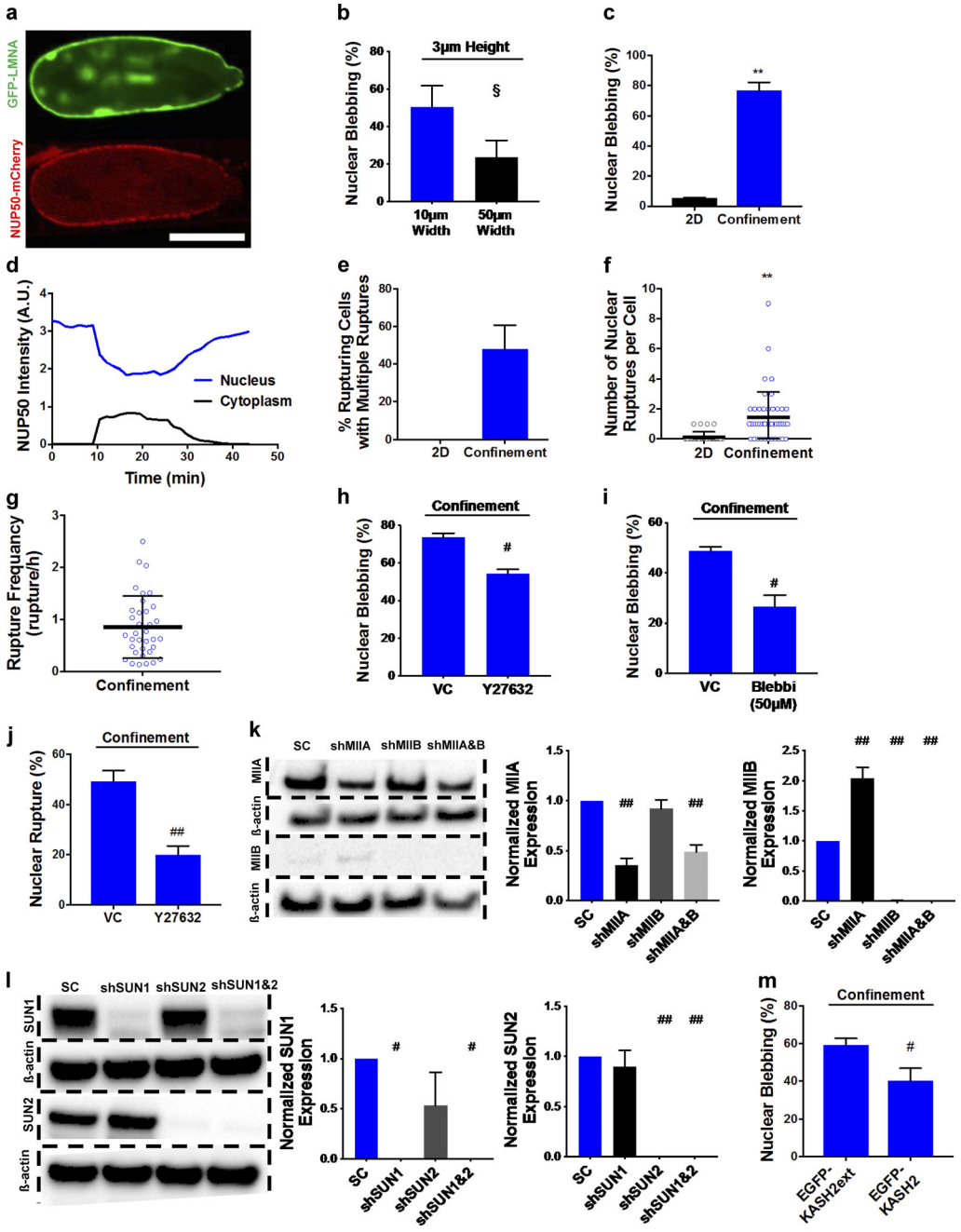

Figure S1. **Confinement-induced RhoA/ROCK/myosin-II–dependent nuclear blebbing and rupture is observed in multiple cancer cell lines. (a)** 60× image of the nucleus of a live HT-1080 cell expressing GFP-LMNA and NUP50-mCherry in confinement. **(b)** Percentage of HT-1080 cells displaying nuclear blebs inside 10-µm- and 50-µm-wide channels with a fixed height of 3 µm (n = 3 independent experiments with a minimum of 15 cells per experiment). **(c)** Percentage of HOS cells exhibiting nuclear blebbing in 2D and confinement (n = 5 independent experiments with a minimum of 20 cells per experiment). **(d)** Quantification of NUP50 signal intensity in the nucleus and the cytoplasm for a representative cell during a nuclear rupture event. **(e)** Percentage of nuclear rupturing-HT-1080 cells that experience more than one rupture event for confined and 2D cells ($n \geq 3$ independent experiments with a minimum of four cells per experiment). **(f)** Number of nuclear rupture events that occur in 2D or confined HT-1080 cells ($n \geq 30$ cells from three independent experiments). **(g)** Frequency of nuclear rupture during confined HT-1080 cell migration (n = 35 cells from three independent experiments). **(h)** Percentage of VC and Y27632-treated HOS cells exhibiting nuclear blebbing in confinement (n = 2 independent experiments with a minimum of 20 cells per experiment). **(i)** Percentage of control and blebbistatin (50 µM)–treated HT-1080 cells displaying nuclear blebbing in confinement, as observed from cells fixed and stained with Hoechst ($n \geq 3$ independent experiments with a minimum of 15 cells per experiment). **(j)** Percentage of VC and Y27632-treated HT-1080 cells experiencing nuclear rupture in confinement, as quantified from mislocalization of NLS-MBP-GFP-NES(Rev) from the cytoplasm to the nucleus (n = 3 independent experiments with a minimum of eight cells per experiment). **(k)** Western blot (left) and quantification (right) of the knockdown efficiency of shMIIA and/or shMIIB (n = 3 independent experiments). Contrast of the entire MIIB blot was enhanced linearly to improve image clarity. **(l)** Western blot (left) and quantification (right) showing the knockdown efficiency of shSUN1 and/or shSUN2 ($n \geq 2$ independent experiments). **(m)** Percentage of EGFP-KASH2ext and EGFP-KASH2 infected HT-1080 cells displaying nuclear blebbing ($n \geq 3$ independent experiments with a minimum of 15 cells per experiment). Values represent mean ± SEM (b, c, e, and h–m) or SD (f and g). §, $P < 0.05$ relative to 10 µm width; **, $P < 0.01$ relative to 2D; #, $P < 0.05$, ##, $P < 0.01$ relative to vehicle/scramble control.

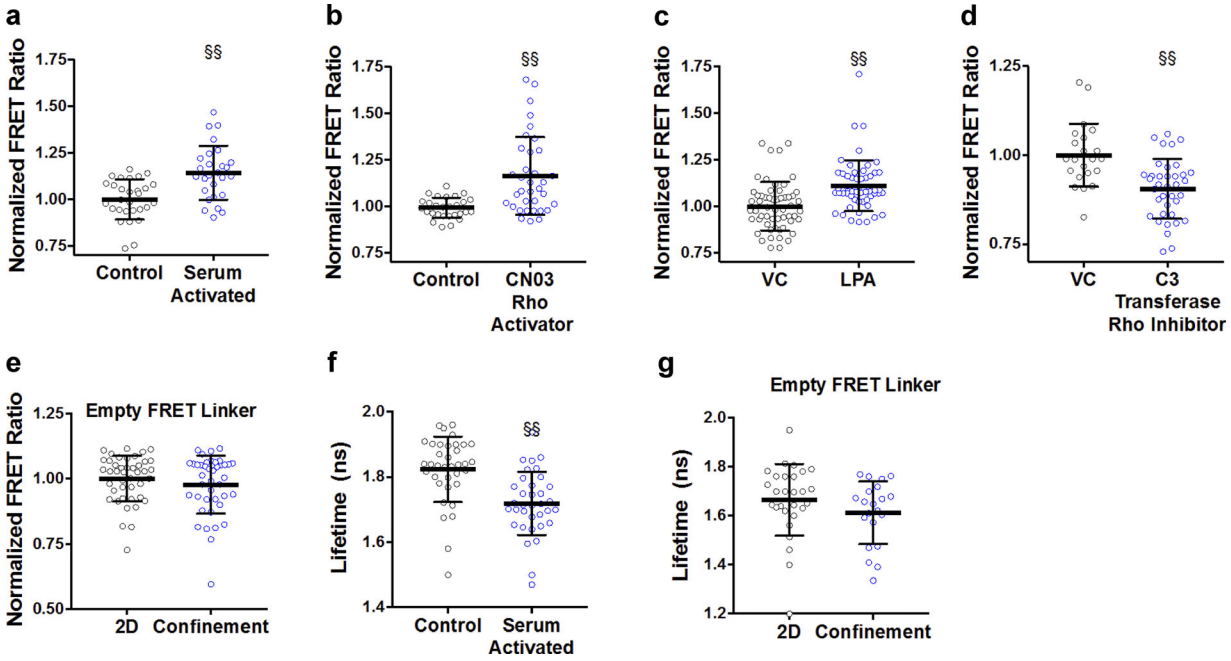

Figure S2. **The RhoA2G biosensor effectively measures RhoA activity. (a–d)** Normalized FRET ratio of RhoA activity biosensor of control, FBS (10%) activated ($n \geq 27$ cells from two independent experiments), CN03 (Rho activator, 1 µg/ml, $n \geq 28$ cells from two independent experiments), lysophosphatidic acid–treated (LPA, 50 µM; $n \geq 18$ cells from two independent experiments), and C3 transferase–treated (Rho inhibitor, 2 µg/ml; $n \geq 22$ cells from two independent experiments) cells plated on 2D surfaces. **(e)** Normalized FRET ratio of empty FRET linker of cells migrating on 2D and inside confined channels ($n \geq 41$ cells from two independent experiments). **(f)** Lifetime of RhoA activity biosensor of control and serum (10%) activated cells ($n \geq 35$ cells from two independent experiments). **(g)** Lifetime of the empty FRET linker of cells migrating on 2D and inside confined channels ($n \geq 21$ cells from two independent experiments). Values represent mean± SD. §§, $P < 0.01$ relative to control or VC.

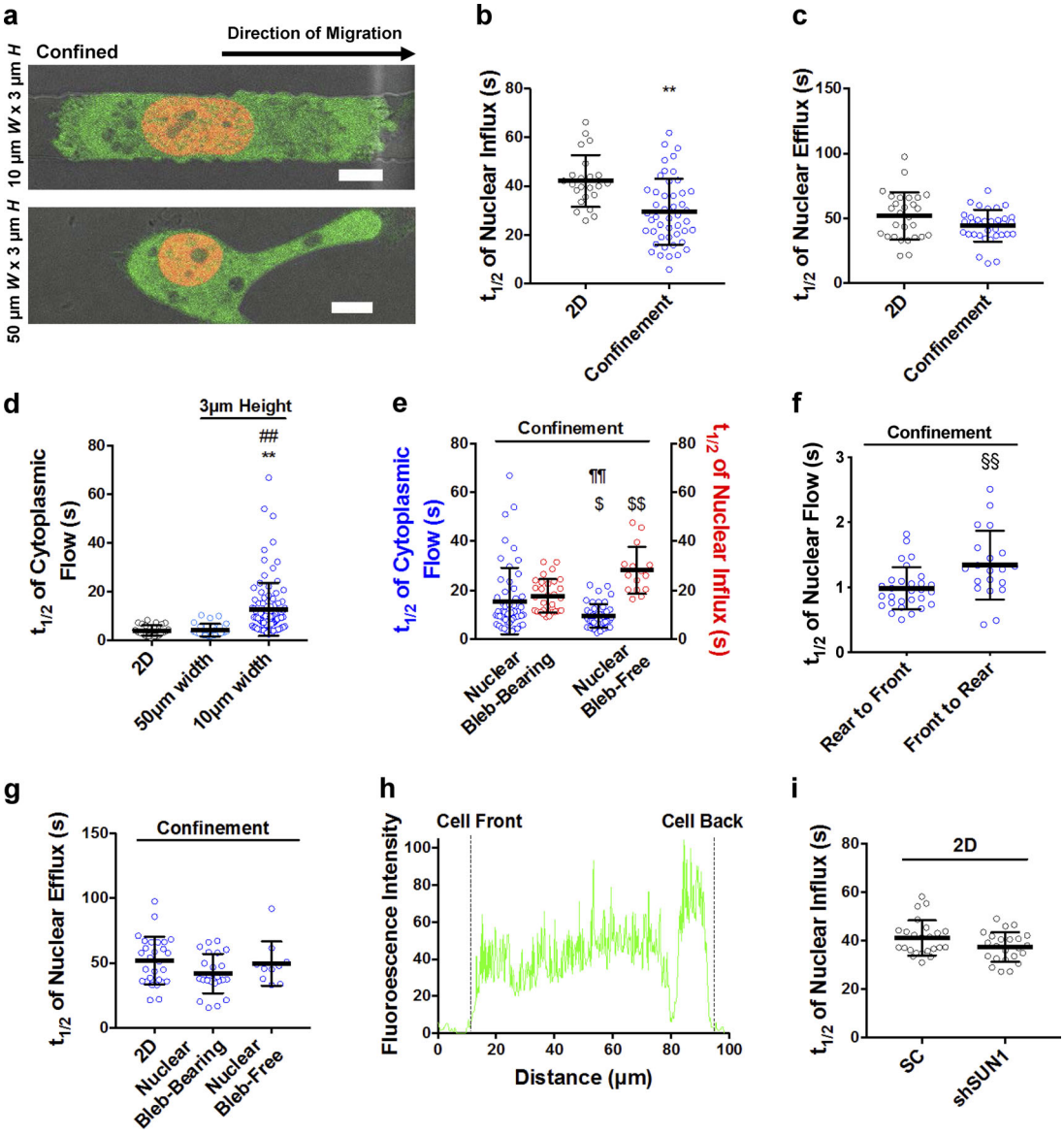

Figure S3. **Nuclear influx, but not efflux, is elevated in confinement. (a)** Image of HT-1080 cells, expressing GFP and H2B-mCherry, demonstrating that the nucleus compartmentalizes the anterior and posterior compartments of the cell in tightly confined channels (10 µm W × 3 µm H; top) but not in wider channels (50 µm W × 3 µm H; bottom). Scale bars, 10 µm. **(b)** $t_{1/2}$ of PA-GFP nuclear influx of HOS cells on 2D or in confinement ($n \geq 23$ cells from three independent experiments). **(c)** Quantification of transport of PA-GFP out of the nucleus (efflux) of HT-1080 cells on 2D or inside confined channels reported as the $t_{1/2}$ required for the signal (PA-GFP) to reach minimum intensity in the nucleus ($n \geq 28$ cells from three independent experiments). **(d)** $t_{1/2}$ of PA-GFP transport from the rear to the front of the cell for HT-1080 cells plated on 2D or migrating in confined channels (10 µm W × 3 µm H) or in wider channels (50 µm W × 3 µm H) ($n \geq 30$ cells from three or more independent experiments). **(e)** $t_{1/2}$ of PA-GFP transport from the rear to the front of the cell as well as nuclear influx for nuclear bleb-bearing and nuclear bleb–free HT-1080 cells in confined channels ($n \geq 15$ cells from three or more independent experiments). **(f)** $t_{1/2}$ of PA-GFP transport from the front to the rear or rear to the front of the nucleus in confined HT-1080 cells ($n \geq 20$ cells from three independent experiments). **(g)** $t_{1/2}$ of PA-GFP nuclear efflux in HT-1080 cells plated on 2D or migrating in confinement with and without nuclear blebs ($n \geq 10$ cells from three independent experiments). **(h)** GFP intensity of cell and surrounding channel space two minutes after simultaneous photoactivation and ablation. **(i)** $t_{1/2}$ of PA-GFP nuclear influx of scramble and shSUN1 cells plated on 2D ($n \geq 23$ cells from three independent experiments). Values represent mean ± SD. **, P < 0.01 relative to 2D; ##, P < 0.01 relative to 50 µm width; $, P < 0.05, $$, P < 0.01 relative to nuclear bleb-bearing; ¶¶, P < 0.01 relative to nuclear bleb-free influx; §§, P < 0.01 relative to rear to front.

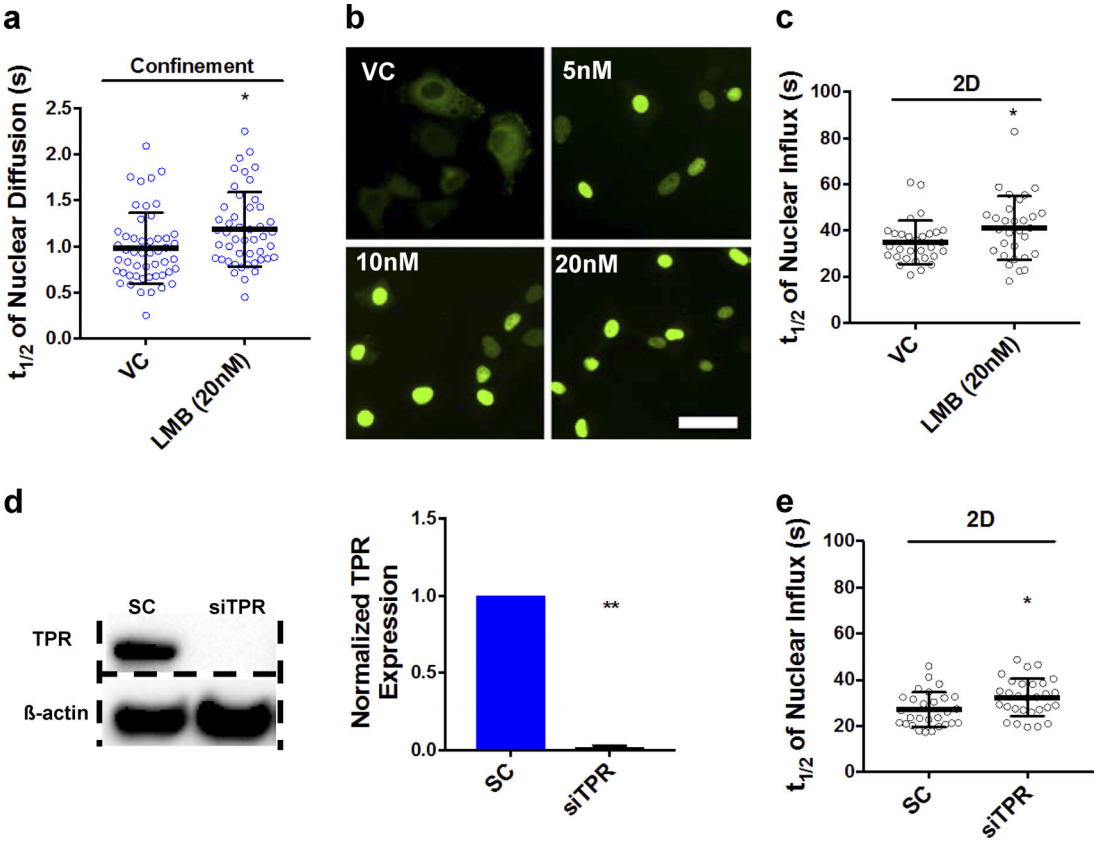

Figure S4. **Nuclear export inhibition reduces passive nuclear efflux by increasing nuclear viscosity. (a)** $t_{1/2}$ of PA-GFP nuclear diffusion for VC and LMB-treated HT-1080 cells in confinement ($n \geq 47$ cells from five independent experiments). **(b)** Image of NLS-MBP-GFP-NES (Survivin) expressing HT-1080 cells treated with vehicle or 5, 10, or 20 nM LMB. Scale bars, 25 µm. **(c)** $t_{1/2}$ of PA-GFP nuclear influx for VC and LMB-treated HT-1080 cells on 2D ($n \geq 30$ cells from three independent experiments). **(d)** Western blot (left) and quantification (right) showing the knockdown efficiency of siTPR ($n = 2$ independent experiments). **(e)** $t_{1/2}$ of PA-GFP nuclear influx for scramble control and TPR-knockdown HT-1080 cells on 2D ($n \geq 28$ cells from three independent experiments). Values represent mean ± SD (a, c, and e) or SEM (d). *, $P < 0.05$, **, $P < 0.01$ relative to VC/SC.

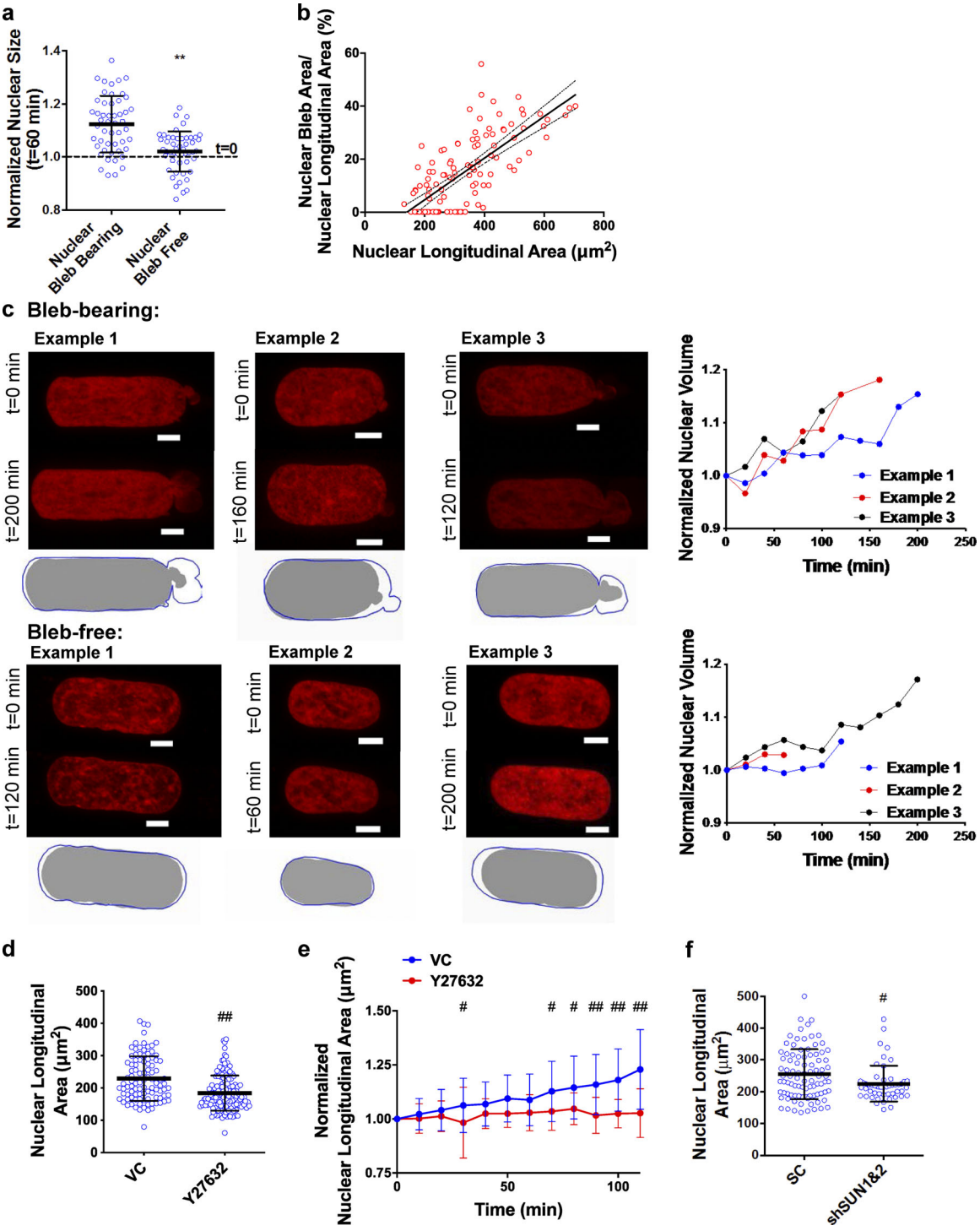

Figure S5. **Nuclear volume increases over time in confinement. (a)** Nuclear longitudinal area of cells with or without nuclear blebs migrating in confinement for 60 min, as quantified from live cells expressing H2B-mCherry ($n \geq 50$ cells from three independent experiments). **(b)** HT-1080 nuclear longitudinal area plotted as a function of the ratio of nuclear bleb area to total nuclear area. Solid line represents the best fit and dotted lines represent the 95% CI ($n = 120$ cells from four independent experiments). **(c)** Representative images and quantification of nuclear volume during migration for nuclear bleb-bearing (top) and nuclear bleb–free (bottom) cells, as measured from confocal Z-stacks of HT-1080 H2BmCherry cells. Gray images and blue outlines represent the maximum intensity projection of the H2B-mcherry labeled nuclei at t = 0 min and t = t_{final}, respectively, for six representative cells. Example 2 (bleb-bearing) quantification matches the bleb-bearing cell quantified in Fig. 5 d. Scale bars, 5 µm. **(d)** Nuclear longitudinal area of VC and Y27632 treated HT-1080 cells in confinement, as measured from live cells expressing H2B-mCherry. **(e)** Nuclear longitudinal area as a function of migration time inside confined channels for VC and Y27632-treated H2B-mCherry-labeled HT-1080 cells ($n = 2$ independent experiments, $n \geq 20$ cells per experiment). **(f)** Nuclear longitudinal area of scramble and SUN1/2-knockdown HT-1080 cells in confinement, as measured from live cells expressing H2B-mCherry. Values represent mean ± SD. **, $P < 0.01$ relative to confined nuclear bleb-bearing; #, $P < 0.05$, ##, $P < 0.01$ relative to vehicle/scramble control.

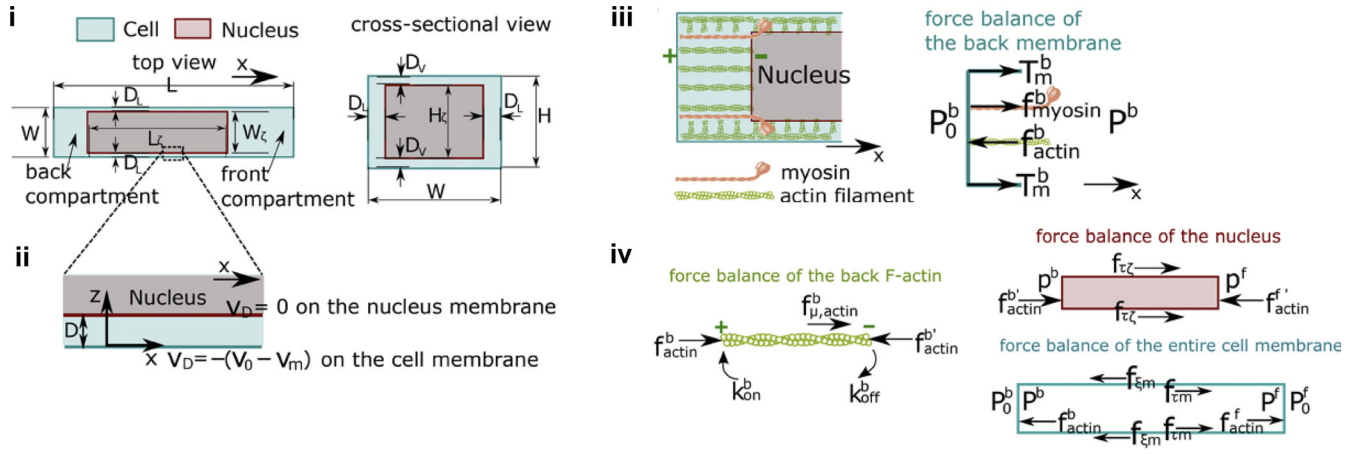

Figure S6. **Schematics explaining the parameters of the mathematical model for the effects of nuclear volume on cell motility. (i)** Geometry of the cell and the nucleus. Confinement: H × W = 3 µm × 10 µm. The nucleus divides the cells into two compartments, one at the front and one at the back. **(ii)** Diagram of the local coordinate system for the flow in the gap between the nucleus and the cell membrane. The generic local coordinate follows the motion of the nucleus. v_0 is the velocity of the nucleus and v_m is the velocity of the lipid membrane of the cell. This coordinate system works for all four gaps around the nucleus. **(iii)** Diagram of the force balance at the back end of the cell membrane. The force balance at the front membrane is similar. **(iv)** Diagram of force balances of the actin filaments at the back of the cell, the entire cell membrane, and the nucleus.